

## Auger decay of 3*p*-ionized krypton

V. Jonauskas, S. Kučas, and R. Karazija

*Institute of Theoretical Physics and Astronomy, Vilnius University, A. Goštauto 12, Vilnius LT-01108, Lithuania*

(Received 2 October 2011; published 15 November 2011)

A theoretical study of Auger cascades during the decay of 3*p*<sub>1/2</sub> and 3*p*<sub>3/2</sub> vacancies in krypton has been performed by level-by-level calculations using a wide configuration interaction basis. Auger spectra for all steps of the cascades are presented and are compared with the existing experimental data. Good agreement of our results with the branching ratios of ions measured by a coincidence technique is obtained.

DOI: [10.1103/PhysRevA.84.053415](https://doi.org/10.1103/PhysRevA.84.053415)

PACS number(s): 32.80.Aa, 32.80.Fb, 32.80.Zb

### I. INTRODUCTION

Auger and radiative cascades following the production of a vacancy in an inner electronic shell of an atom is one of the most complex atomic phenomena. Their investigation gives important information on competing processes during the deexcitation of an atom and many-electron and relativistic effects in the inner shells. The strong impact for the development in this direction was given by the elaboration of coincidence methods for the registration of several particles obtained in the formation of the initial vacancy state and its deexcitation: photoelectron-photoion [1,2], Auger electron-photoion [3,4], Auger electron-photoelectron [5–7], and multielectron spectroscopies [8–10]. This enables disentangling Auger spectra corresponding to different initial vacancy states, providing a more complete insight into the branching of the cascade.

While the cascade in the inner shells of many-electron atoms involves a large number of configurations with open shells and an enormous number of transitions, the average methods for its modeling are often used: the average configuration method [11,12], its extended version (taking other statistical characteristics of spectra into account) [13], or Monte Carlo simulation [14–16]. In such a way, the correspondence to the experimental data for a general characteristic—the distribution of ions in various ionization stages—is often obtained (with some exceptions due to strong correlation effects). However, the reliable interpretation of Auger and radiative spectra generated during the cascade is possible only using high-accuracy level-by-level calculations in configuration interaction (CI) approximation [17–20].

Due to the complexity of such spectra, the commonly considered objects are the atoms of inert gases. The important case of the cascade in the many-electron atom is the decay of the inner vacancy states in krypton. 3*d* Auger decay was the most extensively investigated: the yield spectra of the multiply charged ions [21–23], the many-electron effects during this cascade [24], and the structure of Auger spectra, corresponding to single and double transitions [20,25]. The following step in the investigation of Auger cascades in Kr would be the detailed experimental and theoretical considerations of the more complex cascade after production of the deeper 3*p* vacancy.

In the case of the 3*p* cascade, the distributions of charge states mainly were investigated. This was performed experimentally using the photoelectron-photoion coincidence [21,22], final ion-charge resolving electron spectroscopy, and photoion-Augur electron coincidence [23]. The branching ratios of multiply charged ions were calculated by the

average configuration method [12]; their discrepancy from the experimental data was removed by a detailed calculation of the cascade in CI approximation [24]. Also, the correspondence to the experimental data for ion yields was obtained by Monte Carlo modeling [16].

Only noncoincident  $M_{2,3} - M_{4,5}N_1$ ,  $M_{2,3} - M_{4,5}N_{2,3}$ , and  $M_{2,3} - M_{4,5}N_{2,3}$  Auger spectra associated with both initial vacancies were measured [26]. Any data are absent for one of the main channels of the 3*p* vacancy decay—super-Coster-Kronig transitions  $M_{2,3} - M_{4,5}M_{4,5}$ . The essential role of many-electron effects for the 3*p*<sup>−1</sup> deexcitation process was revealed by the large-scale CI calculations [24]. The aim of our paper is to continue this investigation: to perform the sophisticated large-scale calculations of ion yields and Auger spectra generated during selectively excited 3*p*<sub>1/2</sub> and 3*p*<sub>3/2</sub> cascades in krypton.

### II. THEORETICAL MODEL

The experimental 3*p*<sub>1/2</sub> and 3*p*<sub>3/2</sub> fluorescence yields equal approximately 10<sup>−4</sup>, thus, the radiative transitions can be neglected in the deexcitation of vacancy states. Also, we have not included the shake effect at the production of the initial vacancy because the coincidence experiments enable separating the pure initial state. It was also neglected the additional ionization of an atom during Auger transitions because it plays a less significant role [27], and the condition of sudden perturbation is hardly applicable for such process.

We consider the sequential Auger transitions that go through discrete intermediate states. The energy levels and Auger transition rates have been calculated in the relativistic Dirac-Fock-Slater CI approximation employing the Flexible Atomic Code [28].

The total number of *nl*-configurations used in the calculations for the 3*p*<sub>*j*</sub> cascade was extended essentially in comparison with our earlier paper [24]. In that paper, 64 configurations were taken into account, and the CI effects were not included for the initial vacancy state. In this paper, the sets included the following numbers of *nl*-configurations: 40 for Kr<sup>+</sup>, 128 for Kr<sup>2+</sup>, 139 for Kr<sup>3+</sup>, 129 for Kr<sup>4+</sup>, and 76 for Kr<sup>5+</sup>. The one-electron excitations were taken up to the shells of *n* = 7, whereas, the two-electron excitations included shells up to *n* = 5.

In the lowest order of perturbation theory, the interaction of two levels of different configurations is proportional to the matrix element of Hamiltonian between them and inversely proportional to the energetic distance between these levels.



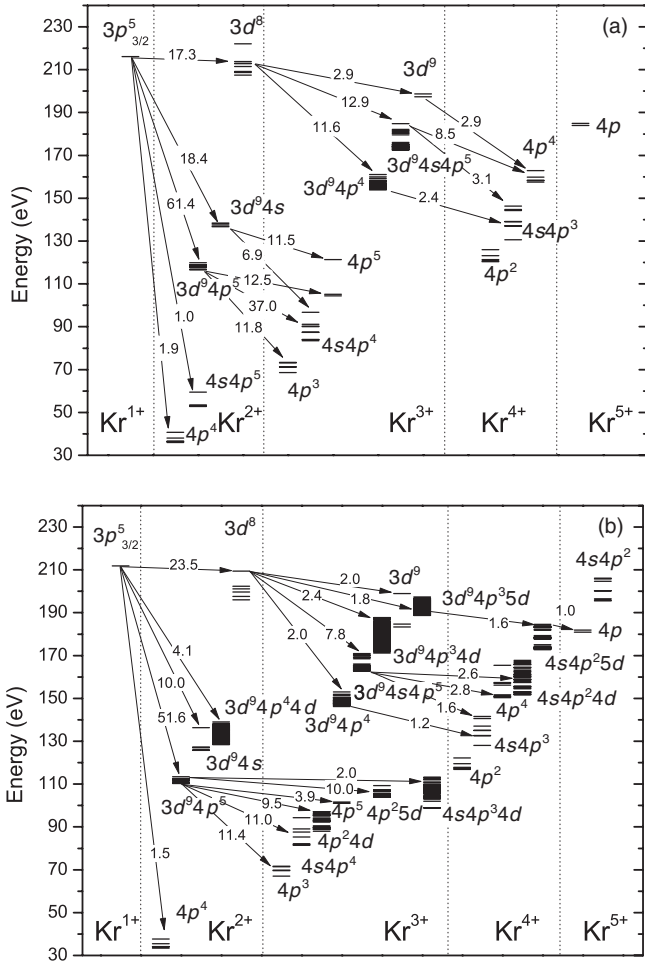


FIG. 2. Auger cascade following the production of the  $3p_{3/2}$  vacancy in Kr, calculated in (a) single configuration and (b) many-configuration approximations. The explications are the same as in Fig. 1.

The additional information on the proceeding of the cascade is given by the lifetimes of decaying states. Their values depend on many-electron quantum numbers: The maximum differences are obtained only when some states of the configuration deexcite through strong Auger transitions to the levels of overlapping configuration or only when radiative deexcitation is possible for some states. The number of levels amounts to several thousand even for the main part of the cascade shown in Figs. 2(a) and 2(b), thus, in Table I, only the average computed lifetimes are given. These quantities obtain the largest values for the initial  $3p_j^{-1}$  states and tend to decrease with the shift of vacancies toward outer shells. Nevertheless, the average lifetimes for some configurations from the further step of the cascade often exceed their values for the configurations from the lower-ionization stage. One reason for a small lifetime is the Auger deexcitation of such a configuration only by mixing with the other configuration. The comparison with the experimental data is possible only for  $3p_{1/2}^{-1}$  and  $3p_{3/2}^{-1}$  levels: Their lifetimes, obtained from the widths of lines ( $\tau_{\text{exp}}(3p_{1/2}^{-1}) = 5.1 \times 10^{-16} \text{ s}$  and  $\tau_{\text{exp}}(3p_{3/2}^{-1}) = 6.0 \times 10^{-16} \text{ s}$  [26]), exceed the calculated values about two times.

TABLE I. Averaged lifetimes for the main configurations taking part in the  $3p$  Auger cascade.

Ion	Configuration	$\tau$ (s)
Kr <sup>+</sup>	$3p_{1/2}^{-1}$	$3.71 \times 10^{-16}$
	$3p_{3/2}^{-1}$	$3.04 \times 10^{-16}$
Kr <sup>2+</sup>	$3d^8$	$4.64 \times 10^{-15}$
	$3d^9 4p^4 4d$	$1.06 \times 10^{-14}$
	$3d^9 4p^4 5d$	$1.30 \times 10^{-14}$
	$3d^9 4p^4 5s$	$1.08 \times 10^{-14}$
	$3d^9 4p^5$	$2.20 \times 10^{-14}$
	$3d^9 4s$	$6.66 \times 10^{-15}$
	$3d^9 5d$	$8.56 \times 10^{-16}$
	$4p^4 4d 6d$	$1.31 \times 10^{-15}$
	$4s 4p^3 4d 5d$	$1.38 \times 10^{-15}$
	Kr <sup>3+</sup>	$3d^9$
$3d^9 4p^3 4d$		$1.94 \times 10^{-14}$
$3d^9 4p^3 4f$		$1.88 \times 10^{-14}$
$3d^9 4p^3 5d$		$2.48 \times 10^{-14}$
$3d^9 4p^3 5s$		$2.06 \times 10^{-14}$
$3d^9 4p^3 6s$		$2.04 \times 10^{-14}$
$3d^9 4p^4$		$2.65 \times 10^{-14}$
$3d^9 4s 4p^5$		$1.55 \times 10^{-14}$
$4p^3 4d 5d$		$1.97 \times 10^{-15}$
$4s 4p^2 4d 5d$		$4.42 \times 10^{-15}$
Kr <sup>4+</sup>	$4s 4p^3 5d$	$5.23 \times 10^{-15}$
	$4s 4p^2 4f$	$2.20 \times 10^{-14}$
	$4s 4p^2 5d$	$1.39 \times 10^{-14}$

During the  $3p$  Auger cascade, ions from Kr<sup>2+</sup> up to Kr<sup>5+</sup> are obtained (Table II). The results of the calculation in the averaged single configuration approximation [12] did not reproduce the experimental data [21,23] at all. This disagreement was removed by taking the main correlation effects [12] into account. The extension of the CI basis in this paper yet improves the correspondence of the theoretical results to the measured values; the largest effect is obtained for Kr<sup>3+</sup> and Kr<sup>4+</sup> yields.

After the Auger cascade, various ions of krypton remain in  $4s^2 4p^N$ ,  $4s 4p^{N+1}$  and  $4s^0 4p^{N+2}$  configurations. Some of these final states are populated by different cascade branches.

Comparison of calculated and known experimental Auger spectra for the first step of the  $3p$  cascade is presented in Figs. 3–5. The lines of the theoretical spectrum were convoluted by a Lorentz profile by only taking their natural width (we neglected the broadening contribution from the electron spectrometer because it was about ten times smaller) into account. The natural width of the lines was calculated as the sum of widths for the initial and final states.

Our calculated spectra were obtained shifted with respect to the experimental spectra to the higher-energy side by about 7.5 eV for the transitions into the final state with  $3d$  vacancy and by about 2.5 eV for the transitions into the states with both  $4l$  vacancies. This difference consists of the positive shift for binding energy (its calculated values:  $I(3p_{1/2}) = 224.2$  and  $I(3p_{3/2}) = 216.0$  eV exceed the experimental data equal to

TABLE II. Branching ratios of Kr ions obtained during the cascades following the production of  $3p_{1/2}^{-1}$  and  $3p_{3/2}^{-1}$  vacancy states.

Initial vacancy	Method	Charge state				
		1+	2+	3+	4+	5+
$3p^{-1}$	Calc <sup>a</sup>	0	3.2	93.8	3.0	0
$3p_{1/2}^{-1}$	Exp <sup>b</sup>	<1	1	55	44	
	Exp <sup>c</sup>	<2(2)	<2(2)	53(3)	44(3)	<2(2)
	Calc <sup>d</sup>	0	2.6	60.9	33.3	3.2
	This paper	0	3.1	54.4	40.9	1.6
$3p_{3/2}^{-1}$	Exp <sup>b</sup>	<1	5	72	23	
	Exp <sup>c</sup>	<2(2)	<2(2)	67(3)	28(2)	<2(2)
	Calc <sup>d</sup>	0	2.9	74.1	21.5	1.5
	This paper	0	3.6	67.8	27.5	1.2

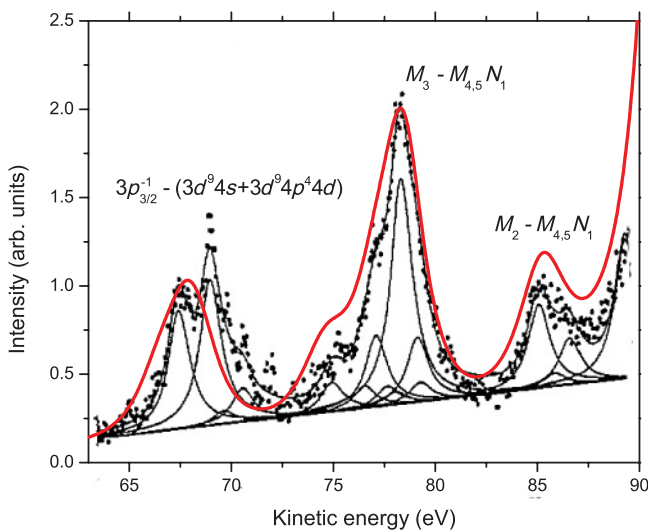
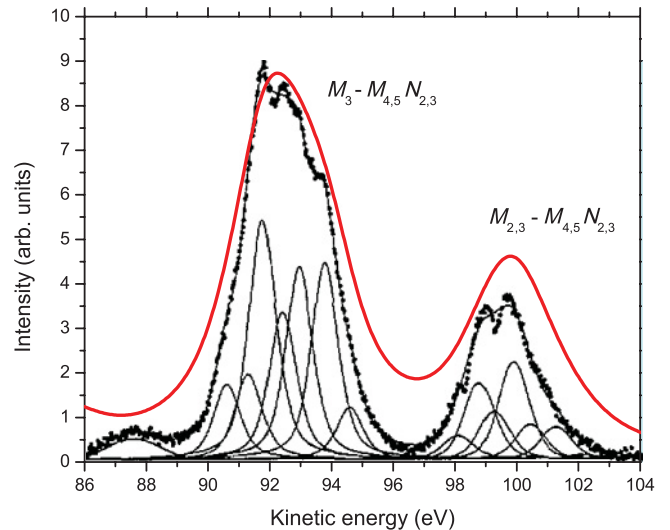
<sup>a</sup>Reference [12].<sup>b</sup>Reference [21].<sup>c</sup>Reference [23].<sup>d</sup>Reference [24].

222.2 and 214.4 eV, respectively [30]) and of the negative shift for the energies of the final states. The main reason probably is the not-included interaction of the autoionizing states with the continuum. At the exclusion of this total shift, the calculated spectra reproduce the experimental spectra fairly well, although the structure of the theoretical maxima is less expressed due to a larger calculated width of the lines.

The large-scale calculations confirm the interpretation of these spectra given in Ref. [26] on the grounds of multiconfiguration Dirac-Fock calculations for transition energies only including several configurations. The CI effects are most significant for the  $M_3 - M_{4,5}N_1$  spectrum, where the CI gives rise to the additional satellite structure around 65 – 70 eV (Fig. 3). The satellite corresponding to the deexcitation of the  $3p_{1/2}^{-1}$  state manifests itself only in the form of a step at 75 eV. The experimental  $M_{2,3} - NN$  spectrum was registered in the interval of 150 – 185 eV, however, its part with better resolution was given only for the narrower region (Fig. 5). The calculated spectrum also contains a distinct

$M_2 - N_{2,3}N_{2,3}$  peak at larger energies as well as an additional peak corresponding to the extended structure of transitions  $3p_{3/2}^{-1} - (4s4p^5 + 4p^34d)$ . The two low-intensity peaks in the 165–170 eV interval can be identified as similar transitions but from the  $3p_{1/2}^{-1}$  state.

The super-Coster-Kronig spectrum  $M_{2,3} - M_{4,5}M_{4,5}$ , corresponding to the transitions  $3p^5 - 3d^8$ , remains unregistered (Fig. 6). It is very sensitive to the location of the  $3d^8$  configuration energy-level spectrum with respect to the initial  $3p_{1/2}^{-1}$  and  $3p_{3/2}^{-1}$  levels. The positions of the  $3d^8$  levels can be estimated from the interpretation of the  $L_{2,3} - M_{4,5}M_{4,5}$  spectrum [31]. However, due to the large natural width of the  $2p$  vacancy state, the transitions to the separate levels, except  $^1S$ , were not resolved. On the grounds of the multiconfiguration Dirac-Fock calculations for the energies of the  $3p^{-1} - 3d^8$  transitions [26] (not presented in that paper), it was concluded that they all were allowed energetically from the  $3p_{1/2}^{-1}$  state but only a smaller part of such transitions were allowed from the lower  $3p_{3/2}^{-1}$  state. Under the assumption

FIG. 3. (Color online) Theoretical and experimental [26] results for the  $M_{2,3} - M_{4,5}N_1$  spectrum.FIG. 4. (Color online) Theoretical and experimental [26] results for the  $M_{2,3} - M_{4,5}N_{2,3}$  spectrum.

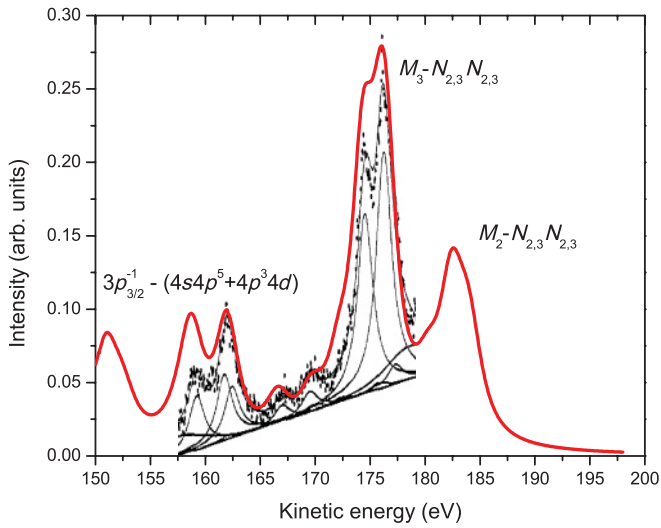


FIG. 5. (Color online) Theoretical and experimental [26] results for the  $M_{2,3} - NN$  spectrum.

that the calculated  $M_{2,3} - M_{4,5}M_{4,5}$  spectrum was shifted in the same amount as the  $M_{2,3} - M_{4,5}N_{2,3}$  spectrum with respect to the experiment, it was suggested that the  $3p^5 - 3d^8$  transitions yet can be forbidden in a greater extent [26]. According to our calculations, all Auger transitions from the  $3p_{1/2}^{-1}$  and  $3p_{3/2}^{-1}$  levels to the levels of the  $3d^8$  configuration are energetically possible. Thus, the experimental registration of the  $M_{2,3} - M_{4,5}M_{4,5}$  spectrum is highly desirable.

The Auger spectra generated during all steps of the  $3p$  cascades are presented in Fig. 7, and the interpretation of their main structure is given in Table III. The spectra of various steps essentially overlap in the region of middle and small energies. The difference in spectra corresponding to the  $3p_{1/2}$  and  $3p_{3/2}$  cascades diminishes with the ionization stage, and for the last step, they practically coincide. Due to the natural width of the lines amounting to 0.5 eV and a small extent of this spectrum, its shape obtains the form of a continuous band. All main lines of this spectrum end in the  $Kr^{5+} 4p$  configuration.

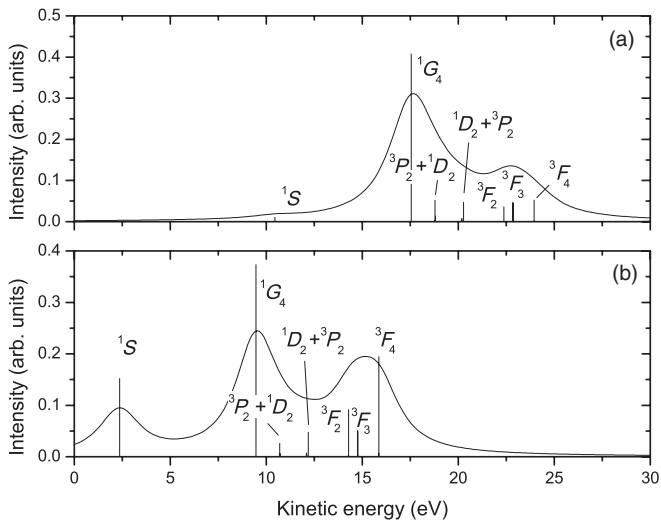


FIG. 6. Theoretical (a)  $M_2 - M_{4,5}M_{4,5}$  and (b)  $M_3 - M_{4,5}M_{4,5}$  spectra.

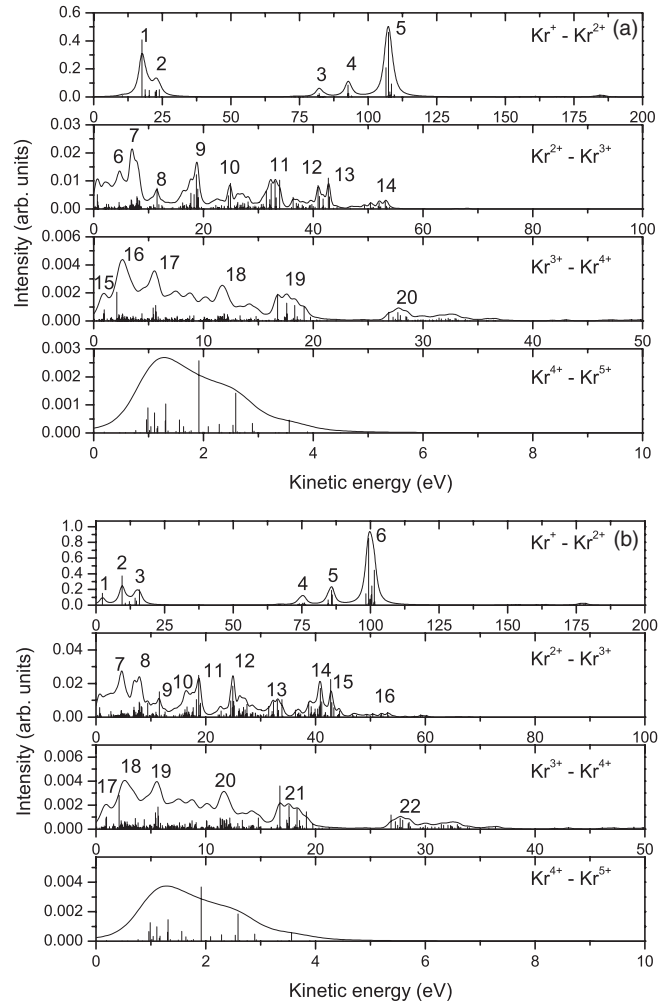


FIG. 7. Auger spectra corresponding to 1–4 steps of (a)  $3p_{1/2}$  and (b)  $3p_{3/2}$  cascades.

The complete Auger spectra of cascades (Fig. 8) are mainly determined by the most intensive transitions of the first step. Even the contribution of the second step almost is undistinguished.

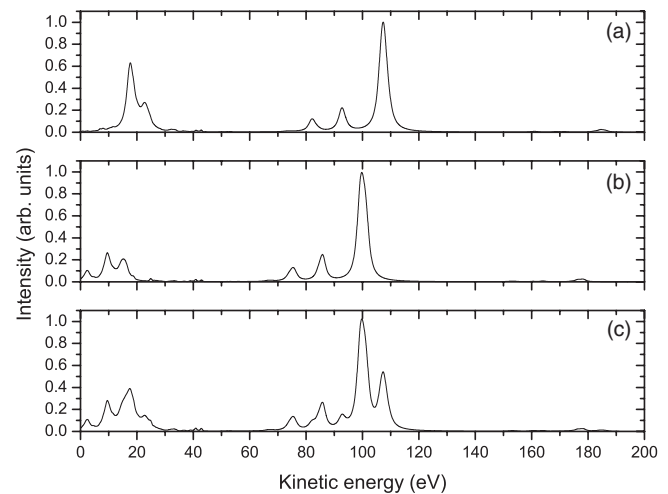


FIG. 8. Complete Auger spectra corresponding to (a)  $3p_{1/2}$ , (b)  $3p_{3/2}$ , and both (c)  $3p$  cascades.

TABLE III. Interpretation of the main Auger spectra lines obtained during the  $3p$  cascade in Kr.

Number	$3p_{1/2}$		$3p_{3/2}$	
	Energy (eV)	Transition	Energy (eV)	Transition
1	17.8	$3p^5 - 3d^8$	2.3	$3p^5 - 3d^8$
2	22.7	$3p^5 - 3d^8$	9.6	$3p^5 - 3d^8$
3	82.2	$3p^5 - 3d^9 4p^4 4d$	15.2	$3p^5 - 3d^8$
4	92.8	$3p^5 - 3d^9 4s$	75.4	$3p^5 - 3d^9 4s + 3d^9 4p^4 4d$
5	107.3	$3p^5 - 3d^9 4p^5$	85.9	$3p^5 - 3d^9 4s$
6	4.7	$3d^9 4p^5 - 4p^2 5d$	99.8	$3p^5 - 3d^9 4p^5$
7	7.0	$3d^9 4s - 4p^2 5d$	4.6	$3d^9 4p^5 - 4p^2 5d$
8	11.5	$3d^9 4p^5 - 4p^5$	7.9	$3d^9 4p^5 - 4p^2 5d$
9	18.8	$3d^8 - 3d^9$ , $3d^9 4p^5 - 4p^2 4d$	11.5	$3d^9 4p^5 - 4s^0 4p^5$
10	24.8	$3d^9 4p^5 - 4p^2 4d$ , $3d^9 4p^5 - 4s 4p^4$	16.5	$3d^9 4p^5 - 4p^2 4d$
11	32.2–33.1	$3d^8 - 3d^9 4s 4p^5$	18.7	$3d^9 4p^5 - 4p^2 4d$
12	41.0	$3d^9 4p^5 - 4p^3$	24.9	$3d^9 4p^5 - 4s 4p^4$
13	42.8	$3d^9 4p^5 - 4p^3$	32.1–33.2	$3d^8 - 3d^9 4s 4p^5$
14	52–53.2	$3d^8 - 3d^9 4p^4$	40.8	$3d^9 4p^5 - 4p^3$
15	0.9	$4s 4p^3 5d - 4p^2$	42.8	$3d^9 4p^5 - 4p^3$
16	2.6	$4s 4p^3 5d - 4p^2$	51.9–53.2	$3d^8 - 3d^9 4p^4$
17	5.6	$4s 4p^3 5d - 4p^2$	0.9	$4s 4p^3 5d - 4p^2$
18	11.7	$3d^9 4s 4p^5 - 4s 4p^2 4d$	2.6	$4s 4p^3 5d - 4p^2$
19	16.8–18.4	$3d^9 4s 4p^5 - 4p^4$	5.6	$4s 4p^3 5d - 4p^2$
20	27.6	$3d^9 4s 4p^5 - 4s 4p^3$	11.6	$3d^9 4s 4p^5 - 4s 4p^2 4d$
21			16.7–18.4	$3d^9 4s 4p^5 - 4p^4$
22			27.8	$3d^9 4s 4p^5 - 4s 4p^3$

#### IV. CONCLUSIONS

The large-scale level-by-level calculations of the  $3p_{1/2}$  and  $3p_{3/2}$  cascades in krypton have been performed taking more than 500 main and admixed configurations with about 110 000 levels into account. The fairly good correspondence to the known experimental data for the ion distribution in different ionization stages and for Auger spectra corresponding to the first step of the cascade is obtained. The largest influence on the branching ratios of both cascades has the strong interaction of configurations  $4s 4p^N + 4s^2 4p^{N-2} 4d$  at the presence or absence of the  $3d$  vacancy.

The super-Coster-Kronig spectrum  $M_{2,3} - M_{4,5} M_{4,5}$  is very sensitive to the energetic positions of the initial and

final states, thus, its modeling remains problematic. The experimental registration of this spectrum is highly desirable. Auger spectra presented in our paper for separate steps of the  $3p_{1/2}$  and  $3p_{3/2}$  cascades can be useful for further investigation by coincidence methods.

#### ACKNOWLEDGMENTS

We gratefully thank Professor H. Aksela and other authors of the Ref. [26] paper for the permission to reproduce the experimental Auger spectra for Kr given there. This work was partly supported by the Research Council of Lithuania, Contract No. MIP-61/2010.

- [1] E. Shigemasa, T. Koizumi, Y. Itoh, T. Hayaishi, K. Okuno, A. Danjo, Y. Sato, and A. Yagishita, *Rev. Sci. Instrum.* **63**, 1505 (1992).
- [2] S. Brünken, C. Gerth, B. Kanngiesser, T. Luhmann, M. Richter, and P. Zimmermann, *Phys. Rev. A* **65**, 042708 (2002).
- [3] D. W. Lindle, W. Les Manner, L. Steinbeck, E. Villalobos, J. C. Levin, and I. A. Sellin, *J. Electron Spectrosc. Relat. Phenom.* **67**, 373 (1994).
- [4] Y. Tamenori, K. Okada, S. Tanimoto, T. Ibuki, S. Nagaoka, A. Fujii, Y. Haga, and I. H. Suzuki, *J. Phys. B* **37**, 117 (2004).
- [5] P. Bolognesi, M. Coreno, A. De Fanis, V. Feyer, S. Turchini, N. Zema, T. Proserpi, and L. Avaldi, in *Auger Electron-Photoelectron Coincidence Experiments in Atomic Collisions*, edited by A. Lahmam-Bennani and B. Lohmann, AIP Conf. Proc. No. 811 (AIP, New York, 2006), p. 138.
- [6] J. Viefhaus, M. Braune, S. Korica, A. Reinköster, D. Rolles, and U. Becker, *J. Phys. B* **38**, 3885 (2005).
- [7] V. Ulrich, S. Barth, S. Joshi, T. Lischke, A. M. Bradshaw, and U. Hergenhahn, *Phys. Rev. Lett.* **100**, 143003 (2008).
- [8] P. Lablanquie, F. Penent, R. I. Hall, H. Kjeldsen, J. H. D. Eland, A. Muehleisen, P. Pelicon, Z. Smit, M. Zitnik, and F. Koike, *Phys. Rev. Lett.* **84**, 47 (2000).

- [9] K. Ito, F. Penent, Y. Hikosaka, E. Shigemasa, I. H. Suzuki, J. H. D. Eland, and P. Lablanquie, *Rev. Sci. Instrum.* **80**, 123101 (2009).
- [10] J. Palaudoux, P. Lablanquie, L. Andric, J. H. D. Eland, and F. Penent, *J. Phys.: Conf. Ser.* **141**, 012012 (2008).
- [11] V. L. Jacobs, J. Davis, B. F. Rozsnyai, and J. W. Cooper, *Phys. Rev. A* **21**, 1917 (1980).
- [12] A. G. Kochur, V. L. Sukhorukov, A. I. Dudenko, and P. V. Demekhin, *J. Phys. B* **28**, 387 (1995).
- [13] R. Karazija, S. Kučas, and V. Jonauskas, *Lith. J. Phys.* **44**, 183 (2004).
- [14] M. O. Krause and T. A. Carlson, *Phys. Rev.* **158**, 18, (1967).
- [15] T. Mukoyama, T. Tonuma, A. Yagishita, H. Shibata, T. Matsuo, K. Shima, and H. Tawara, *J. Phys. B* **20**, 4453 (1987).
- [16] A. H. Abdullah, A. M. El-Shemi, and A. A. Ghoneim, *Radiat. Phys. Chem.* **68**, 697 (2003).
- [17] R. Karazija and S. Kučas, *Sov. Phys. Collect.* **19**(4), 20 (1979).
- [18] F. von Busch, U. Kuetsgens, J. Doppelfeld, and S. Fritzsche, *Phys. Rev. A* **59**, 2030 (1999).
- [19] V. Jonauskas, L. Partanen, S. Kučas, R. Karazija, M. Huttula, S. Aksela, and H. Aksela, *J. Phys. B* **36**, 4403 (2003).
- [20] J. Palaudoux, P. Lablanquie, L. Andric, K. Ito, E. Shigemasa, J. H. D. Eland, V. Jonauskas, S. Kučas, R. Karazija, and F. Penent, *Phys. Rev. A* **82**, 043419 (2010).
- [21] S. Brünken, C. Gerth, B. Kanngiesser, T. Luhmann, M. Richter, and P. Zimmermann, *Phys. Rev. A* **65**, 042708 (2002).
- [22] T. Matsui, H. Yoshii, A. Higurashi, E. Murakami, T. Aoto, T. Onuma, Y. Morioka, A. Yagishita, and T. Hayaishi, *J. Phys. B* **35**, 3069 (2002).
- [23] Y. Tamenori, K. Okada, S. Tanimoto, T. Ibuki, S. Nagaoka, A. Fujii, Y. Haga, and I. H. Suzuki, *J. Phys. B* **37**, 117 (2004).
- [24] V. Jonauskas, R. Karazija, and S. Kučas, *J. Phys. B* **41**, 215005 (2008).
- [25] E. Andersson, S. Fritzsche, P. Linusson, L. Hedin, J. H. D. Eland, J.-E. Rubensson, L. Karlsson, and R. Feifel, *Phys. Rev. A* **82**, 043418 (2010).
- [26] J. Jauhiainen, A. Kivimäki, S. Aksela, O.-P. Sairanen, and H. Aksela, *J. Phys. B* **28**, 4091 (1995).
- [27] S. Brühl and A. G. Kochur, *J. Phys. B* **43**, 105002 (2010).
- [28] M. F. Gu, *Can. J. Phys.* **86**, 675 (2008).
- [29] S. Kučas, V. Jonauskas, and R. Karazija, *Phys. Scr.* **55**, 667 (1997).
- [30] *X-Ray Data Booklet*, Center for X-ray Optics and Advanced Light Source (Lawrence Berkeley National Laboratory, Berkeley, 2009), [<http://xdb.lbl.gov>].
- [31] L. O. Werme, T. Bergmark, and K. Siegbahn, *Phys. Scr.* **6**, 141 (1972).